Functional Evaluation of an Artificial Anal Sphincter Using Shape Memory Alloys

YUN LUO,* TOSHIYUKI TAKAGI,* TAKESHI OKUYAMA,* SHINTARO AMAE,† MOTOSHI WADA,† KOTARO NISHI,† TAKAMICHI KAMIYAMA,† TOMOYUKI YAMBE,‡ AND HIDETOSHI MATSUKI§

This article describes an implantable artificial anal sphincter using shape memory alloys and its *in vivo* assessment in porcine models. The new design was developed as a low invasive prosthesis with a simple structure to solve the problem of severe fecal incontinence in patients with hypoplastic sphincters or without anal sphincters and especially for ostomates. The artificial anal sphincter consists of two shape memory alloy (SMA) plates as the main functional parts to perform two basic functions when the SMA artificial sphincter is fitted around intestines (*i.e.*, an occlusion at body temperature and an opening function on heating). Our previous assessments with short-term animal experiments revealed promising properties with the occlusion function of the device, although some complications, such as overpressure induced ischemia, heat burn, and infections, remained. This article addresses the concerns related to the practical use of the device, the power supplement to drive the actuator, and overheating protection of the device inside bodies. Results of chronic animal experiments of up to 4 weeks suggested great potential for the improved device. *ASAIO Journal* 2004; 50:338–343.

Incontinence, generally classified into urinary incontinence and fecal incontinence, has negative physical, psychologic, social, and economic effects on patients. Medical treatments, such as surgical reproduction of a neosphincter or electrical stimulation, have proved effective for selected patients. Artificial urinary sphincters have been developed and implanted in patients and have had a high success rate.[1,2] Meanwhile, little attention has been given to research on artificial anal sphincters. Prostheses with a structure similar to an inflatable circular cuff fitted around the anorectal bowel have been developed and studied in both animal experiments and clinical trials.[3–9] These implantations have improved incontinence, but they remain a controversial treatment, mainly because of reported mechanical failure and structures using a liquid drive mechanism. In addition, to be proportional to the dimension of the intestines, larger sizes of the cuff, balloon, and pump are required.

We proposed a novel artificial anal sphincter with a simple structure using shape memory alloys (SMAs). The purpose of this work was to reduce the number of parts of the device and to develop a compact design for a less invasive prosthesis.[10–12]

SMAs are functional materials with the unique characteristics of the shape memory effect (SME) and pseudo elasticity (PE). The features in the mechanical behavior of SMA materials, the high ratio of recovery force to weight, and large recoverable strains enable their applications for various compact actuators and sensors in industrial products, daily appliances, and medical applications.[13,14] The use of SME allows freedom in the design of medical actuators such as artificial muscles,[15] active catheters,[16] and SMA valves for urinary incontinence.[17] The commercialized artificial sphincter AMS-800 consists of three actuation required parts: an inflatable silicone cuff, a pressure regulating balloon, and a manual pump. The proposed artificial anal sphincter has only one deformable part (*i.e.*, the artificial sphincter itself), which is, therefore, expected to reduce the possibility of mechanical failure.

Our previous results from animal experiments on the preliminary evaluation of the SMA artificial anal sphincter showed promising properties for the occlusion of intestines.[11,12] However, postoperative complications and thermal burn were observed in tissues around the implanted device. The reasons for the problems have been attributed to the percutaneous lines connected to the external power supply and a lack of an overheating control in the device. In the current study, we made improvements (1) to decrease the potential for infection by incorporating a transcutaneous energy transmission (TET) system to realize complete implantation, thereby eliminating the potential for infection, and (2) to develop a thermal control inside bodies. Results of chronic animal experiments with the improved device are reported.

Materials and Methods

A typical SMA material with two way shape memory effect (TWSME), Ti51at%Ni, was adopted in this work. SMA plates were subjected to a solution treatment (850°C, 20 minutes) followed by an aging treatment (400°C, 100 hours) with restrained arc shapes. The transformation temperatures were measured by the differential scanning calorimetry (DSC) technique. At temperatures higher than body temperature, the material revealed only transformations between a rhombohedral phase (R-phase) and an austenite phase (A-phase). The start and finish temperatures are obtained by DSC measure-

From the *Institute of Fluid Science, Tohoku University, †Graduate School of Medicine, Tohoku University; ‡Institute of Development, Aging and Cancer, Tohoku University; and §Graduate School of Engineering, Tohoku University.

Submitted for consideration July 2003, accepted in revised form April 2004.

Correspondence: Yun Luo, Tohoku University Biomedical Engineering Research Organization, 2-1 Seiryo, Aoba-ku, Sendai 980-8575, Japan, e-mail: luo@tubero.tohoku.ac.jp

DOI: 10.1097/01.MAT.0000131819.07741.EF

ments: A_s' = 47°C, A_f' = 52°C for A-phase and M_s' = 49.5°C, M_f' = 44.5°C for R-phase.

A schematic drawing of the proposed artificial anal sphincter is shown in **Figure 1**. The actuator consists of two SMA plates jointed by hinges at their ends and foil type heaters attached on the SMA plates. Each SMA plate is 65 mm long, 15 mm wide, and 0.7 mm thick. Silicone pillows are placed on the surfaces of the SMA plates to prevent the pressure concentration on intestines that causes ischemia. Another function of the silicone pillows is for thermal insulation, because the highest temperature for the complete reverse transformation of the SMA might be higher than Af', although the maximum tolerable temperature for tissues of living bodies is approximately 42°C. The artificial sphincter can be fitted around intestines and act with an occlusive force on the intestines at body temperature. On heating, the reverse R-phase transformation occurs in the SMA plates, accompanied by the shape changes from a flat shape to an arc shape. The shape change results in a lumen between two SMA plates, which allows bowel movement. After switching off the electrical power for heating, the SMA plates recover to their initial shapes on natural cooling, closing the intestines again. A prototype of the developed artificial sphincter is shown in **Figure 2**. It is 80 mm long, 15 mm wide, and 20 mm high. The SMA material in its rhombohedral phase, which exists at body temperature, has a lower Young's modulus than that in its austenite phase, and is easy to deform mechanically. This characteristic enables another function for healing the intestines after the implantation. If we deform the SMA ribbons to arc shapes to have a lumen in the artificial sphincter, this open state would be maintained as long as the SMA artificial sphincter is deactivated. After several days, thermal activation or deactivation can be used to open or close the intestines.

The power to heat the SMA plates can be provided percutaneously by a DC/AC external power supply, but in our previous animal experiments, it was difficult to avoid infection along the electrical lines.[11] The TET system, a technology developed for the power supply of artificial hearts,[18] was then adopted for our artificial anal sphincter. Integrating the TET systems into the SMA actuator can facilitate the complete implantation of an artificial anal sphincter and can eliminate the potential for infection.

The basic design of the device has two elements implanted inside the body: an SMA based artificial sphincter and a secondary coil. Although the former has a comparable dimension to the silicone cuff in the AMS-800, the latter is disklike and drastically reduces the volume of the implant. This promotes the new device as a low invasive prosthesis. In addition, the simple mechanism of the driving principle of the device is expected to enhance its reliability and durability.

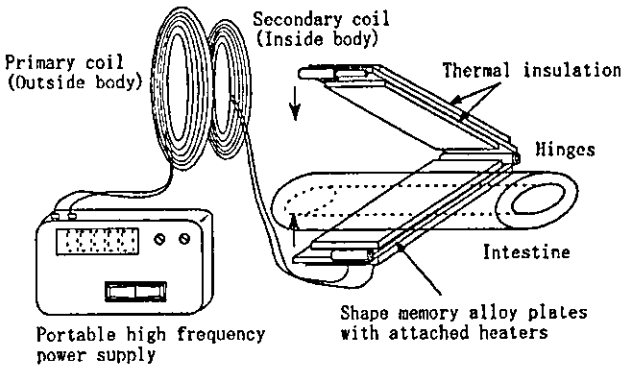

Figure 1. Schematic drawing of the proposed artificial anal sphincter using shape memory alloy.

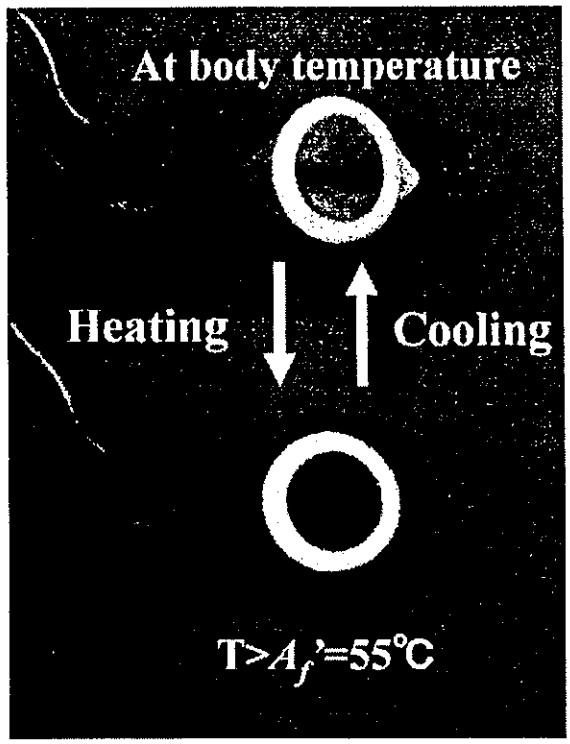

Figure 2. A prototype of the proposed artificial anal sphincter clipping an artificial intestine (upper) and deformed for releasing function (bottom). T, temperature; A_f', finish temperature of reverse transformation.

Results and Discussion

Deformation Under Thermal Cycles

The thermomechanical properties were investigated to determine the maximum obtainable gap between the middle points of two deformed SMA plates large enough to allow a bowel movement. The gap was indirectly evaluated by measuring the strain on the surfaces of the SMA plates. The temperature dependence of the strain is presented in **Figure 3**. As seen in **Figure 3**, on heating, the strain increases slightly from the 43°C because of the local transformation and exhibits a sharp rise from 47°C, corresponding to the start temperature of the reverse transformation, followed by saturating at a maximum value of strain. On cooling until the temperature decreases to the start temperature of the R-phase transformation, the strain remains at the maximum value. The time for this temperature drop allows for the bowel movement. In addition, complete shape recovery was obtained when the temperature dropped to the initial value. The maximum strain ϵ has the relation with the curvature ρ for a specific thickness t, $\epsilon = t/2\rho$. Therefore, for the maximum strain of 1.2% and thickness of 0.7 mm, the curvature is calculated to be approximately 30 mm.

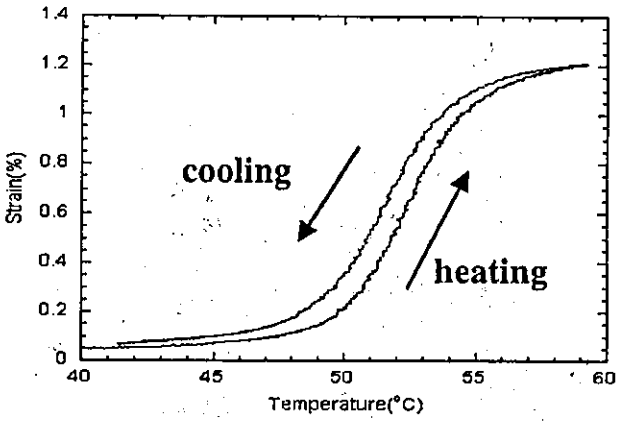

Figure 3. Transformation accompanied strain changes in a Ti51 at %Ni plate underwent a aging treatment with a restrained shape.

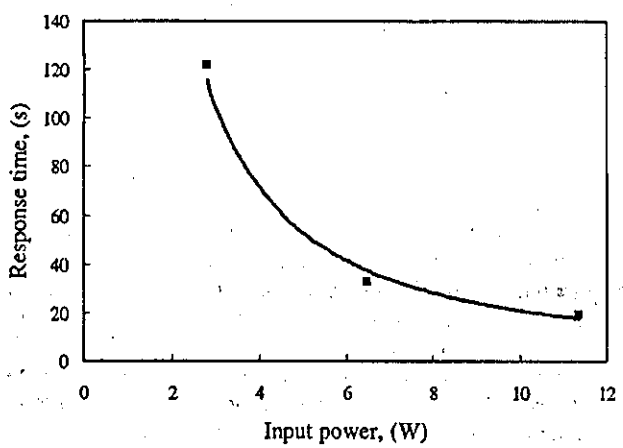

Figure 4. Input power dependences of the response time in an *in vivo* experiment.

The initial strain of the SMA plates is generated by the silicone pillows attached on their inner surfaces. The maximum strain leads to a lumen between two SMA plates of around 30 mm. The practical lumen for opening the intestines should subtract the thickness of silicone pillows 10 mm (5 mm for each one). This lumen was proved adequate for providing appropriate pressure on intestines in our animal experiments. For clinical trials in the future, this lumen should be set to fit the dimension of the intestines of individual patients through a careful design, taking into account the mechanical interaction between the SMA ribbons, silicone pillows, and natural intestines.

Transient Thermal Responses of the Artificial Sphincter

In our previous study, *in vitro* investigations were conducted on the time response of SMAs and the temperature dependent occlusive properties.[11] At room temperature, the artificial anal sphincter exhibited a good occlusive function against hydrostatic pressures of up to 75 mm Hg, although the mean inner pressure of intestines is estimated to be around 50 mm Hg for human bodies. *In vivo* experiments were performed in the current work to investigate the relationship between the input electrical power and response time. Preliminary tests were carried out, heating the SMA plates from the body temperature to around 60°C by a DC power supply. The transient temperature of the SMA plates was measured by a thermocouple sandwiched between SMA plates and thermal insulations. The input voltage of the power supply was set to 8 V, 12 V, and 16 V for three cases. Because the electrical resistance of the heaters is 22 Ohm, the power for each case becomes 2.9 W, 6.5 W, and 11.5 W. As shown in **Figure 4**, the time responses were 122 seconds, 33 seconds, and 19 seconds for corresponding cases. To obtain a shorter response time, more power is required. The temperatures on the contacting surfaces of the silicone pillows with intestines (inner surface) and the surrounding tissues (outer surface) were measured by thermocouples for confirmation purposes because surface temperatures of the device should be maintained lower than the maximum tolerance value of tissues, 42°C. **Figure 5** shows the results of a representative case with electrical power of 6.48 W (0.54 A, 12 V) and 33 seconds for heating. The power was applied to heat the SMA plates to 60°C and then switched off. The response time was found to be around a half minute. Slight temperature rises were observed on the inner and outer surfaces, but the highest temperatures were lower than 40°C. The peak of the temperature rises on surfaces appeared with a time delay compared with that of SMA plates because of transient heat conduction. The difference in their responses is attributed to the difference in the thickness of thermal insulations: 3 mm for the outer surface and 4 mm for the inner.

Transcutaneous Energy Transmission System

To power implantable devices, TET systems are most suitable for achieving complete implantation, thereby reducing the potential for postoperative infections that are usually difficult to avoid in applications with percutaneous power supply leads. Ventricular assist devices are well known applications of the TET system.[19–21] A typical TET system setup consists of an AC power supply connected with a primary coil providing an alternating field and a secondary coil in which the AC current can be induced and coupled with a load.

For medical applications of TET systems, the thermal effect of

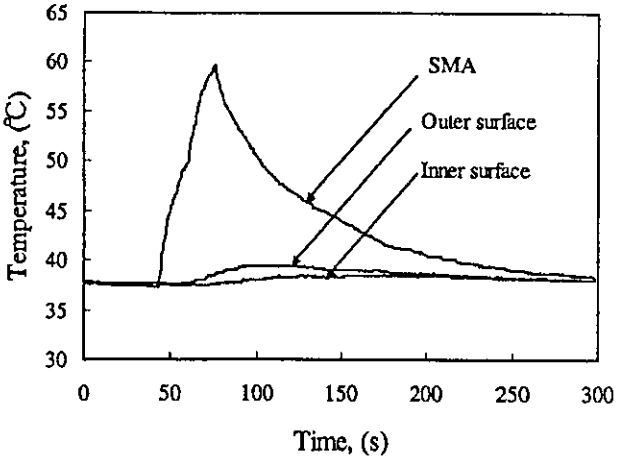

Figure 5. Thermal response of the artificial anal sphincter in an *in vivo* experiment. SMA, shape memory alloy.

the implanted secondary coil on the contacting tissues should be taken into account. Enhancement of energy transfer efficiency is also a common concern in this technology. The thermal effect of the coils on the contacting tissues should be lower than 42°C by reducing the electrical resistance of the coils.[20] However, the optimization of the profile of coils to obtain higher energy transfer efficiency depends on many factors, such as the distance between the primary and secondary coils (defined as coil separation) and the materials of the coil core. A detailed discussion on these topics is beyond the focus of this article. Here we investigated the possibility of power transmission to drive the artificial anal sphincter with adequate coil separations for practical uses. The system, with its block diagram illustrated in **Figure 6**, consists of a high frequency power supply connected to the primary coil L1, a secondary coil L2 connected to the SMA artificial anal sphincter, and spacers with corresponding thickness sandwiched between two disc shaped coils. The coils were made from a twisted bunch of 100 thin copper wires, each with diameter of 0.1 mm. The primary coil has 10 turns of the bunch and has outer and inner diameters of 60 mm and 30 mm. The secondary coil has 8 turns, and its outer and inner diameters are 40 mm and 20 mm. Preliminary experiments have been demonstrated *in vitro* for three cases with the coil separations being 5 mm, 10 mm, and 15 mm. The power with a frequency of 100 kHz was applied in the primary coil with 15 V, 18 V, and 22 V for each case. The power factors depend on the configuration of the experimental setup (here, mainly the coil separation); therefore, the values of power obtained in the coils increase with the decrease of coil separations, and the obtained efficiency exhibits a similar tendency as that seen in **Figure 7**. In a case with a coil separation of 15 mm, the energy transfer efficiency is 56%, and it increases to 70% for a coil separation of 10 mm and to 88% for 5 mm. For a case with a coil separation of 10 mm, which is comparable with cases in practice and power of 10 W, the response time is shorter than half a minute.

In summary, although in animal experiments the secondary coil is implanted under skin with a distance ranging from 5–8 mm from the primary coil, the developed TET system exhibits a capability in energy transfer to the artificial anal sphincter with the coil separations over a range of 5–15 mm with satisfactory responses.

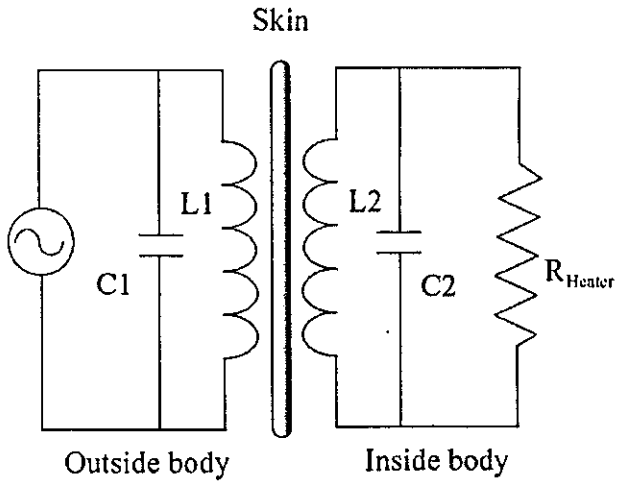

Figure 6. Schematic drawing of a transcutaneous energy transmission system for driving the artificial anal sphincter (indicated by R_{Heater}). L1, primary coil; L2, secondary coil; C1, primary capacitor; C2, secondary capacitor.

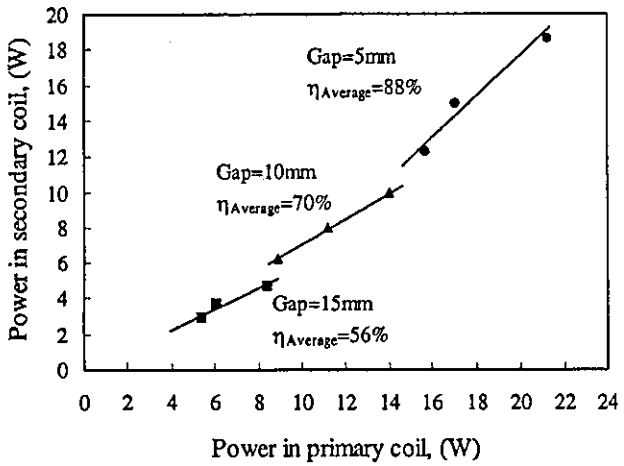

Figure 7. Gap dependency of energy transmission efficiencies with different coil gaps.

Thermal Control

As previously mentioned, a simple switch off control of the applied power can prevent the SMA plates from overheating after a complete deformation. With the maximum temperature being controlled, the temperatures on the contacting surfaces of the silicone pillows with intestines (inner surface) and the surrounding tissues (outer surface) were controlled successfully to be lower than the maximum tolerance value of tissues, 42°C. Because there is no deformation in the temperature range from Af to the start temperature of R-phase transformation Ms, the deformed shape could be maintained for a short period as long as the temperatures were higher than Ms. However, the short period, usually less than 1 minute, was not long enough for the bowel movement. This concern motivated us to develop an approach to control the temperature of SMA plates at around Af, automatically, to elongate the open time without overheating the surrounding tissues.

For this purpose, we introduced a temperature sensitive reed switch (normally closed) into the electrical circuit of the inside part of the device. The switch consists of two permanent magnets and a thermal sensitive ferrite tube, forming a magnetic circuit. A ferromagnetic contacting pair closes normally under a balance between an elastic force and a magnetic force induced by the magnetic field. Heating the ferrite tube reduced its magnetization, and as the temperature exceeded its Curie point, the magnetization dropped to zero, leading to the opening of the magnetic circuit. Without the magnetic force, the contacting pair was opened by the elastic force. It is expected that such a switch will be used to perform on–off control of power applied in the artificial sphincter. The best way is to use a switch directly attached on the SMA to control its temperatures. However, the size of commercially those available inhibits such a design. In this work, an additional heater was used to heat the reed switch. The switch was electrically connected with the SMA sphincter in series. A schematic

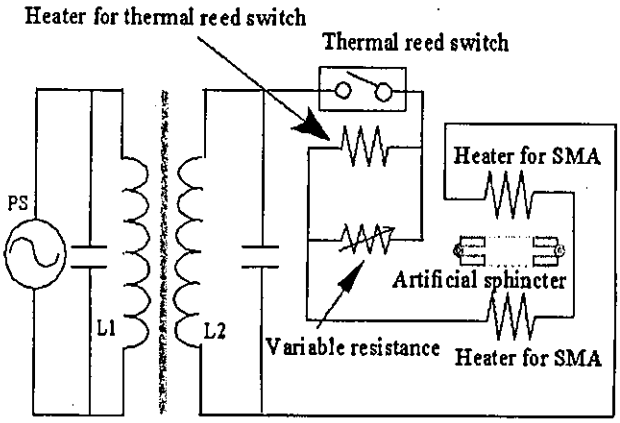

Figure 8. Schematic drawing of the electrical circuit of the proposed system. SMA, shape memory alloy.

drawing of the proposed set is illustrated in **Figure 8.** A thermal sensitive reed switch with a 55°C operating temperature was adopted in the control circuit. To ensure the temperature of the SMA plates could be controlled at A_s', a variable resistor, connected with the additional heater in parallel, was used to bypass the current in the reed switch. Experiments for the confirmation of the proposed approach were conducted. To confirm the robustness of the control scheme, a demonstration of the temperature responses under a variation of applied power was conducted, with a fixed value of the variable resistor. Results of the cases with applied voltage of 15 V and 25 V are shown in **Figure 9.** In each case, the temperature of the reed switch was successfully controlled with an on–off switching at approximately the operating temperature of 55°C. Meanwhile, the average temperature of the SMA plates was successfully controlled at approximately 60°C. This suggests that once the overheating of the SMA plates is controlled, the surface temperatures of the artificial sphincter can be controlled below a certain value by increasing the thickness of the thermal insulation materials. An *in vivo* example is shown in **Figure 10;** the temperature of SMA plates was successfully controlled within a range from 58°C to 65°C, which ensures

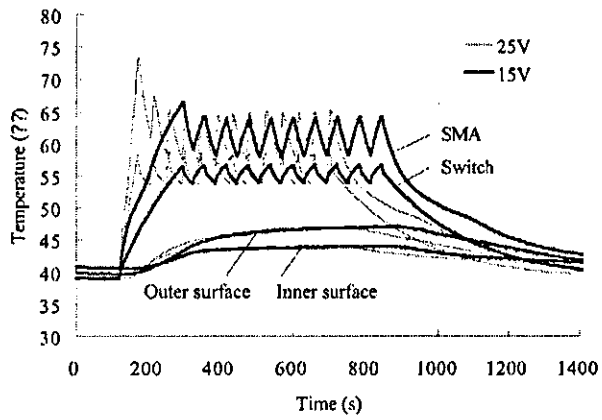

Figure 9. Temperature responses of the shape memory alloy (SMA) plates, the reed switch, and surfaces of the artificial sphincter with applied voltages of 25 V and 15 V.

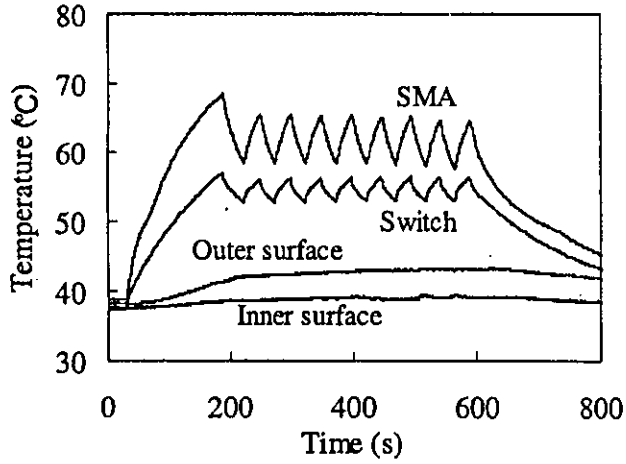

Figure 10. Thermal responses of the artificial sphincter inside the body but with corrected parameters. SMA, shape memory alloy.

the open function of the artificial sphincter. During the operating period of 10 minutes, the surface temperatures did not exceed 43°C. The inner surface, defined as the contact area with the intestines, was found to be much lower than the outer surface because of the difference in the thickness of the thermal insulation. A further reduction of the surface temperatures of the artificial sphincter can be realized easily by increasing the thickness of insulation materials covering the SMA plates.

Animal Experiments

A series of animal experiments, including acute and chronic experiments, were performed on porcine models with weights ranging from 15 kg to 20 kg. All animal experiments were performed with permission issued by the Committee on Animal Experiments in Tohoku University. In our acute experiments, basic functions of the artificial sphincter (*e.g.*, the open occlusion function, the resting anal pressure after implantation, and the thermal behavior of the device) were investigated. Chronic experiments were conducted in two stage operations: a colostomy on the abdomen through the oblique muscles, followed by implantation of the artificial anal sphincter. The colostomy before the implantation of the device is a procedure conducted only to create a situation of complete fecal incontinence in animal models rather than a necessary preoperation to implant the device. For the practical use of the device, the colostomy would, of course, not be required. So, even though this protocol is very invasive, the device itself should not be considered invasive because of the colostomy. In a previous paper, we reported preliminary results on two animal models.[11] Although the occlusion function as a sphincter was completely confirmed with a maximum pressure of 55 mm Hg, severe postoperative complications were found. Problems observed in these experiments were then improved with the new design. For example, the incorporation of the TET system is expected to eliminate postoperative infections and the overheating protector to reduce the thermal impact on surrounding tissues.

With the improved devices, we performed three chronic animal experiments. Two lasted 2 weeks, and one lasted 4 weeks. The occlusion pressures were measured after each implantation. Average values were found ranging from 40 mm Hg to 50 mm Hg. In the former two experiments, without overheating protection, activation of the device was performed

by a simple on–off operation of the power supply. Although at the beginning, fecal continence was regularly observed, constipation was found several days after operation. A possible reason was considered to be the relatively short open time of around 1 minute, which may be not enough for complete evacuation. This problem was solved in the latest experiment. By incorporating the thermal controller into the device, the open time was lengthened to 10 minutes. During the 4 weeks of the experiment, fecal movements were regularly observed when the artificial anal sphincter was activated, and the evacuated feces was confirmed as being normal by comparing with that of controls. At autopsy, postoperative infection was found in a pocket containing the thermal controller, perhaps because of some failure of the silicone coating. Slight burns were found on the surfaces of tissues contacting with the secondary coil and the side face of the artificial sphincter, where the thermal insulations are relatively thin. Nevertheless, neither ischemic anomaly nor heat burn was found in tissues that underwent occlusion pressure most of the time, suggesting the good functionality of the developed artificial anal sphincter.

Conclusion

In summary, an SMA artificial anal sphincter actuated by a TET system has been developed for complete implantation. The use of Ti51 at %Ni, which exhibits TWSME, enables a compact design with simple structure. Fundamental thermomechanical behaviors of the SMA actuator have been investigated in both *in vivo* and *in vitro* experiments. Satisfactory occlusion and release functions of the artificial sphincter were confirmed. Thermal control using a thermal sensitive reed switch was incorporated into the device to prevent the temperature of the SMA plates from overheating. This approach proved effective, allowing a long enough open time of the artificial sphincter for evacuation, and the overheating protection was found to be robust against possible changes in the values of the applied power. The developed SMA artificial sphincter has been implanted in animal models for chronic experiments of up to 4 weeks and has exhibited good performance in maintaining fecal continence.

Results obtained in the current work suggest the possibility of the SMA artificial anal sphincter as a new solution for severe fecal incontinence. However, the assessment of its biocompatibility requires longer animal experiments. Concerning the biocompatibility of materials used in the current work, the TiNi SMAs may give rise to a problem of the possible dissolution of Ni, which is considered toxic. It was reported that an adequate surface treatment such as laser surface melting could dramatically increase the corrosion resistance of the alloys.[22] Moreover, coating the TiNi alloy with polyurethanes followed by 2-methacryloyloxy ethyl phosphorylcholine (MPC) polymers[23] that have been proven to have good biocompatibility should be effective in resisting the corrosion of Ni and making the device biocompatible. In our future work, long-term animal experiments with the SMA artificial anal sphincter implanted will be repeated to confirm the biocompatibility of the device.

Acknowledgement

This research was supported by the Industrial Technology Research Grant Program in 2000 (00A45027) from the New Energy and Industrial Technology Development Organization (NEDO) of Japan.

References

1. Hajivassiliou CA: A review of the complications and results of implantation of the AMS artificial urinary sphincter. *Eur Urol* 35: 36–44, 1999.
2. Petrou SP, Elliott DS, Barrett DM: Artificial urethral sphincter for incontinence. *Urology* 56: 353–359, 2000.
3. Christiansen J, Lorentzen M: Implantation of artificial sphincter for anal incontinence. *Lancet* 1: 244–245, 1987.
4. Lehur PA, Michot F, Denis P, *et al:* Results of artificial sphincter in severe anal incontinence. Report of 14 consecutive implantations. *Dis Colon Rectum* 39: 1352–1355, 1996.
5. Hajivassiliou CA, Carter KB, Finlay IG: Assessment of a novel implantable artificial anal sphincter. *Dis Colon Rectum* 40: 711–717, 1997.
6. Vaizey CJ, Kamm MA, Gold DM, Bartram CI, Halligan S, Nicholls RJ: Clinical, physiological, and radiological study of a new purpose-designed artificial bowel sphincter. *Lancet* 352: 105–109, 1998.
7. Lehur PA, Roig JV, Duinslaeger M: Artificial anal sphincter: Prospective clinical and manometric evaluation. *Dis Colon Rectum* 43: 1100–1106, 2000.
8. Lehur PA, Frank Z, Michel N, Pascal G, Stanislas BV: Comparison of quality of life and anorectal function after artificial sphincter implantation. *Dis Colon Rectum* 45: 508–513, 2002.
9. Hajivassiliou CA, Carter KB, Finlay IG: Biomechanical evaluation of an artificial anal sphincter prosthesis. *J Med Eng Technol* 21(3–4): 89–95, 1997.
10. Takagi T, Luo Y, Hara S, *et al:* An artificial sphincter using shape memory alloy actuators. *Journal of Advanced Science* 12: 337–342, 2000.
11. Amae S, Wada M, Luo Y, *et al.* Development of an implantable artificial anal sphincter by the use of the shape memory alloy (SMA). *ASAIO J* 47: 346–350, 2001.
12. Luo Y, Takagi T, Amae S, *et al:* An SMA artificial anal sphincter actuated by transcutaneous energy transmission systems. *Materials Transactions* 43: 1052–1056, 2002.
13. Kapgan M, Melton KN: Shape memory alloy tube und pipe couplings in Duerig TW, Melton KN, Stockel D, Wayman CM (eds.), *Engineering Aspects of Shape Memory Alloys.* London; Boston: Butterworth-Heinemann, 1990, pp. 137–148.
14. Ohkata I, Suzuki Y. The design and shape memory alloy actuators and their applications in Otuska K, Wayman CM (eds.), *Shape Memory Materials.* Cambridge: Cambridge University Press, 1998, pp. 240–266.
15. Maruyama S, Kawase M, Sakai S, *et al:* Proposal of thermoelectric actuator and development of active catheter. *JSME International Journal,* Series B 43(4): 712–718, 2000.
16. Park K, Lim G, Sugihara M, Minami K, Esashi M: Future of active catheters. *Sensors and Actuators A: Physical* 56(1–2): 113–121, 1996.
17. Chonan S, Jian ZW, Tani J, *et al:* Development of an artificial urethral valve using SMA actuators. *Smart Materials and Structures* 6: 410–414, 1997.
18. Mitamura Y, Hirano A, Okamoto E, Mikami T: Development of transcutaneous energy transmission system, in Akutsu T (ed.), *Artificial Heart-2.* Tokyo, Japan: Springer, 1988, pp. 265–270.
19. Weiss WJ, Rosenberg GR, Snyder AJ, Pae WE, Richenbacher WE, Pierce WS: *In vivo* performance of a transcutaneous energy transmission system with the Penn State motor driven ventricular assist device. *ASAIO Transactions* XXXV: 284–288, 1989.
20. Mussivand T, Miller JA, Santerre PJ, *et al:* Transcutaneous energy transfer system performance evaluation. *Artificial Organs* 17: 940–947, 1993.
21. Mussivand T, Holmes KS, Hum A, Keon WJ: Transcutaneous energy transfer with voltage regulation for rotary blood pumps. *Artif Organs* 20: 621–624, 1996.
22. Villermaux F, Tabrizian M, Yahia L'H, Meunier M, Piron DL: Excimer laser treatment of NiTi shape memory alloy biomaterials. *Applied Surface Science* 109/110: 62–66, 1997.
23. Ishihara K: Bioinspired phospholipid polymer biomaterials for making high performance artificial organs. *Science and Technology of Advanced Materials* 1: 131–138, 2000.

Available online at www.sciencedirect.com
SCIENCE DIRECT®
Biomedicine & Pharmacotherapy 57 (2003) 83s–86s
BIOMEDICINE & PHARMACOTHERAPY
www.elsevier.com/locate/biopha

Can personality traits predict pathological responses to audiovisual stimulation?

Tomoyuki Yambe [a,*], Makoto Yoshizawa [b], Shin Fukudo [c], Hiroshi Fukuda [d], Ryuta Kawashima [e], Kazuhiko Shizuka [a], Shunsuke Nanka [a], Akira Tanaka [f], Ken-ichi Abe [f], Tomonori Shouji [g], Michio Hongo [g], Kouichi Tabayashi [h], Shin-ichi Nitta [a]

[a] *Department of Medical Engineering and Cardiology, Institute of Development, Aging and Cancer, Tohoku University, 4–1 Seiryo-machi, Aoba-ku, Sendai 980–stH5, Japan*
[b] *Information Synergy Center, Tohoku University, Sendai, Japan*
[c] *Department of Behavior Sciences, Tohoku University Graduate School of Medicine, Sendai, Japan*
[d] *Department of Nuclear Medicine and Radiology, Institute of Development, Aging and Cancer, Tohoku University, Sendai, Japan*
[e] *New Industrial Creation Hatchery Center, Tohoku University, Sendai, Japan*
[f] *Tohoku University Graduate School of Engineering, Sendai, Japan*
[g] *Department of Psychosomatic Medicine, Tohoku University Graduate School of Medicine, Sendai, Japan*
[h] *Department of Cardiovascular Surgery, Tohoku University Graduate School of Medicine, Sendai, Japan*

Received 28 July 2003

Abstract

The "Pockemon shock" is the most famous accident in the history of the broadcasting industry in Japan. Based on the experiences of this unfortunate accident from famous animation program "Pocket Monster", this study focused on the psychology and psychosomatics of the patients. A head-mounted display was used as the three-dimensional image presentation device and "Descent", a free software shooting game, was used as the software. Ten healthy adult male volunteers were used in this experiment after obtaining their informed consent. The oxygen metabolic change in the anterior lobe of the brain was measured by near infrared spectroscopy and recorded on an electrocardiogram. The mental scaling tendency of the object was analyzed using the type A behavior pattern and the hostility scaling. The Cook and Medley hostility (HO) scale from the Minnesota multiphasic personality inventory (MMPI) was also used in this experiment. From this scaling methodology, the paranoid scale, cynicism scale, lie scale, social support quality and social support quantity were calculated. All measured time series data were kept in the normal range, and no fatal arrhythmia or epilepsy were observed during experiments. In some cases, the brain oxygen metabolism may completely differ for the objects of Type A and Type B behavior patterns. On the whole, correlation did not become significant in type A scaling and hostility scaling. In a comparison of the percent changes of the HF in HRV with lie scaling, significant negative correlation was observed. The social support quantity was calculated from Cook and Medley, and significant negative correlations were observed with percent changes of LF/HF in HRV. The lie scale and social support quantity are opposite scaling. The sympathetic nervous system and parasympathetic nervous system have an opposite function also. Therefore, our results showed an interesting phenomenon, when considering the relationship between the autonomic function and the pathophysiological reaction to the audiovisual stimulations. As for the photo sensitive epilepsy, it was reported to be only 5–10% for all patients. Therefore, 90% or more of the cause could not be determined in patients who started a morbid response. The results in this study suggest that the autonomic function was connected to the mental tendency of the objects. By examining such directivity, it is expected that subjects, which show morbid reaction to an audiovisual stimulation, can be screened beforehand.

Keywords: Heart rate variability (HRV); Virtual reality (VR); Type A behavior pattern; Hostility scale; Social support quantity

* Corresponding author. Tel.: +81-22-717-8514/8517; fax: +81-22-717-8518.
E-mail address: yambe@idac.tohoku.ac.jp (T. Yambe).

doi:10.1016/j.biopha.2003.08.010

1. Introduction

The "Pockemon shock" is the most famous accident in the history of the broadcasting industry and audiovisual equipment society in Japan [1]. After it happened, the Japanese people started countermeasures immediately. A project team was inaugurated in the several agencies. In Japan, Animation and Television games are progressing at the world's fastest rate. The performance of audiovisual equipment is also No. 1 in the world. The Japanese people regarded the problem to be so serious that they supported the research work on the study for evaluating the responses to audiovisual stimulation such as TV, game machines and newly developed virtual reality (VR) machines [1–4]. In Tohoku University, the autonomic nervous system responding to VR was evaluated [2].

Among the large number of people watching the TV program "Pocket monster", only a small number showed a pathological reaction, but it is necessary to determine the factors for such pathological reaction. This paper focused on the psychology and psychosomatics of the patients [5–8].

2. Materials and methods

An analysis method from the perspective of multiple dimensions is required to analyze a living body response toward VR. A head-mounted display was used as the three-dimensional image presentation device for VR and "Descent", a free software shooting game, was used as the software for the virtual three-dimensional game. In the game, the game player flies in the three-dimensional virtual space, striking down one enemy one after another through movement. The movement of the head does not correspond with the rotation of the view in the three-dimensional image.

An unpleasant sensation is thus created because input to the central nervous system does not correspond with the three-dimensional images. It is well known that a pathological response is started by this game.

Ten healthy adult male volunteers were used in this experiment after obtaining their informed consent approved by the Ethical committee in Tohoku University Graduate School of Medicine.

During the three-dimensional game with VR, the oxygen metabolic change in the anterior lobe of the brain was measured by near infrared spectroscopy (NIRO-300, Hamamatsu Photonics) [9,10]. An electrocardiogram was recorded at the same time to evaluate the heart rate variability (HRV).

The time series data were recorded in the digital data recorder. After the experiments, recorded data were inputted into the personal computer system through the AD converter. Quantified evaluation and statistical handling were performed in the personal computer system. Spectral analysis was performed with fast Fourier transform to evaluate the fluctuations in the time series data.

The mental scaling tendency of the object was analyzed using the type A behavior pattern and the hostility scaling. The Cook and Medley hostility (HO) scale from the Minnesota multiphasic personality inventory (MMPI) was used in this experiment. From this scaling methodology, the paranoid scale, cynicism scale, lie scale, social support quality and social support quantity were calculated.

Responses to the three-dimensional shooting game were compared with the mentality tendency by the quantified value of scaling.

3. Results

All measured time series data were kept in the normal range, and no fatal arrhythmia or epilepsy were observed during experiments. Satisfactory measurements were obtained during experiments in 10 subjects.

Examples of the time series data of a volunteer, who showed a type A behavior pattern, is presented in Fig. 1. Examples of the time series data of a volunteer, who showed a type B behavior pattern, are presented in Fig. 2.

A volunteer with type A behavior showed stable time series data during the three-dimensional VR shooting game in oxygen metabolism of the anterior lobe of the brain. However, the example of a volunteer with type B behavior showed significant alteration in the time series data of oxygen metabolism in the brain.

Responses to the three-dimensional VR game were calculated with percent changes of the heart rate and tissue oxygenation index (TOI) measures with near infrared spectroscopy. Type A behavior scaling and hostility scaling were

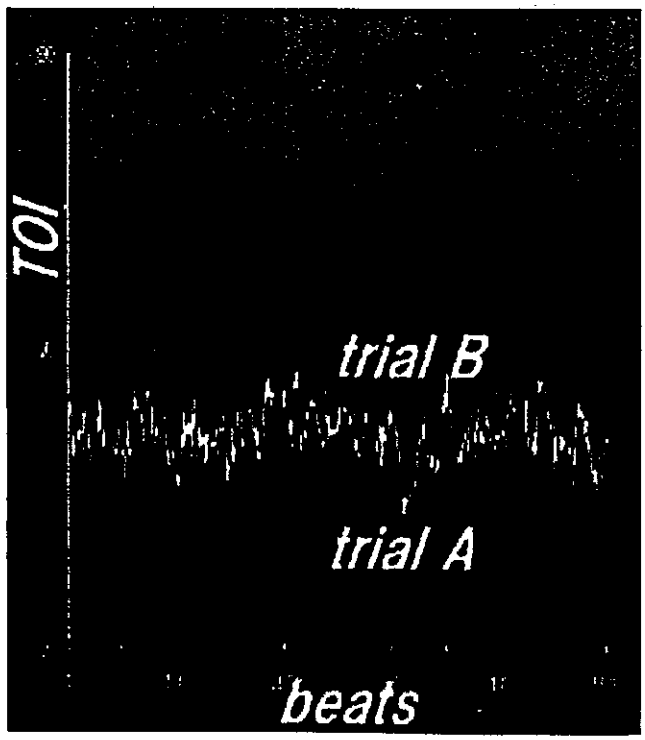

Fig. 1. An example of the time series data of a volunteer, who showed a type A behavior pattern during resting condition and VR game immersion. Trial A showed the data from first experience of this game and trial B showed the second.

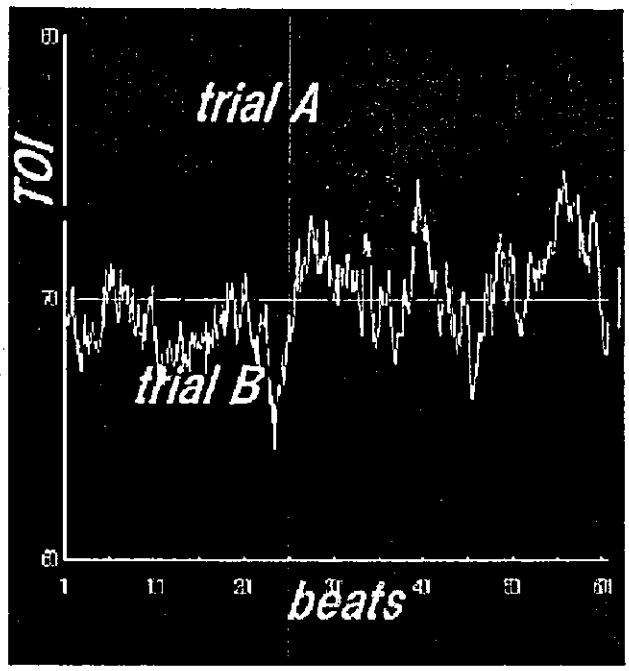

Fig. 2. An example of the time series data of a volunteer, who showed a type B behavior pattern during resting condition and VR game immersion. Trial A showed the data from first experience of this game and trial B showed the second.

calculated and compared with the percent changes of these parameters. However, no significant correlation was observed.

HO scale showed the hostility scale, paranoid scale, cynicism subscale, lie scale and several kinds of social support scaling. These scalings were compared with the percent changes of the parameters, and the lie scale showed significant negative correlation with the percent changes of the heart rate during an experiment.

Spectral analysis was performed for the HRV, LF and HF, and LF/HF were calculated from the analyzed data. Fig. 3 shows the percent changes of the HF in HRV with lie scaling. Significant negative correlation was observed.

The social support quantity was calculated from Cook and Medley. Fig. 4 showed correlation with the percent changes of LF in HRV. Significant negative correlation was calculated.

4. Discussion

It is estimated that over 10 million people watched the Pocket Monster television program in 1997. Among these watchers, over 700 children were taken to hospital by ambulance with severe sickness. It is possible that more children went to hospital by car or on foot—the government does not know the exact number.

It is also possible that the occurrence rate of children, who felt nauseous during the Pocket Monster program, was not so large. Though the percentage may not have been so high, severe convulsions were reported in some patients; thus, the problem was regarded as serious.

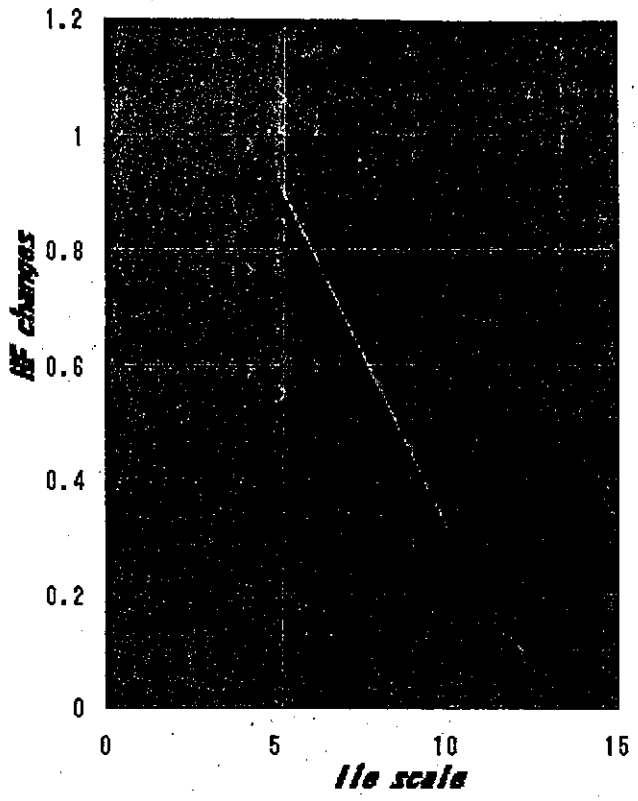

Fig. 3. Relationship between the percent changes of the HF in HRV and lie scaling. Significant negative correlation was observed.

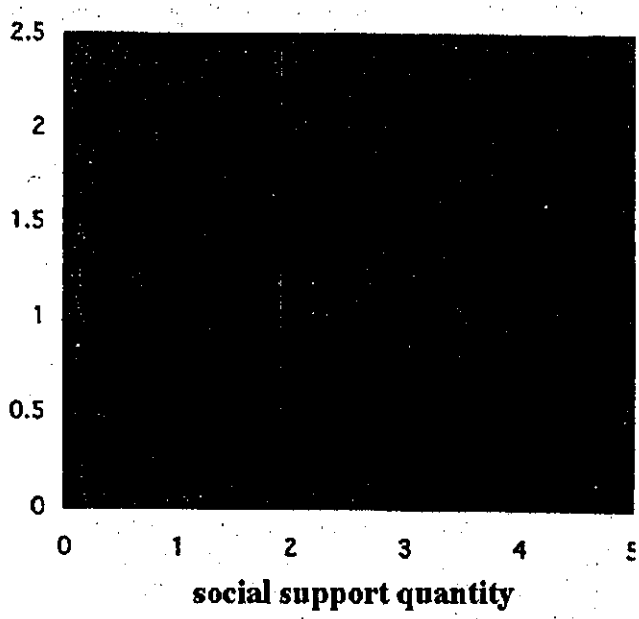

Fig. 4. Relationship between the percent changes of the LF/HF in HRV and social support scaling. Significant negative correlation was observed.

As for the photo sensitive epilepsy, it was reported to be only 5–10% for all of the patients. Therefore, 90% or more of the cause could not be determined in patients who started a morbid response.

What divided the television viewers?

This paper focused on mental characteristics.

In this research, the technique of mental scaling was newly introduced. For mental scaling, the type A behavior pattern and the hostility scaling were used. Various experts have reported on the relevance of a type A behavior pattern and a hostility scaling.

In some cases, the brain oxygen metabolism may completely differ for the object of Type A and Type B behavior patterns. On the whole, correlation did not become significant in type A scaling and hostility scaling. There is argument regarding the relation of the hostility scale and the type A behavior pattern among Japanese people. This concerns the various kinds of low rank scaling in the hostility scaling. Various scaling, such as a cynicism scale, a paranoid scale, a lie scale and a social support quantity, have been reported. Generally, a paranoid scale, a cynicism scale, a lie scale, etc. suggest the directivity of a comparatively negative reaction. A social support quantity is a scale in which an opposite direction is shown.

Significant correlation was observed in the low rank measure of a hostility scaling. Correlation with the lie scale, which is a low rank measure of a hostility scaling, was suggested as the spectrum component of the HRV at the time of the VR game. As for the HRV, the social support quantity also showed significant correlation, too.

The lie scale in Cook and Medley showed a tendency for negative reaction to the responses. The HF component in HRV showed the parasympathetic function. So, the results in this study suggest that the object, which shows a negative reaction, has the high reactivity of a parasympathetic nervous system to the audiovisual stimulation.

The social support quantity is a scale in which an opposite reaction is shown. Generally, the social support quantity is low when the hostility scale is large. LF/HF in HRV showed the sympathetic nerve function. So, results in this study suggest that the object, which shows a positive reaction, has the high reactivity of a sympathetic nervous system to the audiovisual stimulation.

The lie scale and social support quantity are opposite scaling. The sympathetic nervous system and parasympathetic nervous system have the opposite function also. So, our results showed an interesting phenomenon, when considering the relationship between the autonomic function and the pathophysiological reaction to the audiovisual stimulations.

These results suggest that the autonomic function in the three-dimensional game by the VR was connected to the mental tendency of the objects. By examining such directivity, it is expected that subjects that show the morbid reaction to an audiovisual stimulation can be screened beforehand.

After establishing standard guidelines for audiovisual content risks, mental scaling of an object may become an important factor in the future.

Acknowledgements

The authors thank Mr. Kimio Kikuchi for experimental preparation and kind cooperation, Miss Yoko Ito, and Mrs. Hisako Iijima for their excellent technical assistance and kind cooperation.

This work was partly supported by a Grant-in-aid for Scientific Research (11480253), Research Grant for Cardiovascular Diseases from the Ministry of Health and Welfare and Program for Promotion of Fundamental Studies in Health Science of Organizing for Drug ADR Relief, R&D Promotion and Product Review of Japan.

References

[1] Available from: http://www.csicop.org/si/2001-05/pokemon.html.
[2] Yambe T, Yoshizawa M, Nanka S, Sugiyama Y, Mano T, Takayasu H, et al. Responses of the autonomic nervous system to the virtual reality immersion. Proceed for VSMM96 in Gifu. 1996. p. 274–7.
[3] Jang DP, Kim IY, Nam SW, Wiederhold BK, Wiederhold MD, Kim SI. Analysis of physiological response to two virtual environments: driving and flying simulation. Cyberpsychol Behav 2002;5(1):11–8.
[4] Haier RJ, Siegel Jr BV, MacLachlan A, Soderling E, Lottenberg S, Buchsbaum MS. Regional glucose metabolic changes after learning a complex visuospatial/motor task: a positron emission tomographic study. Brain Res 1992;570:134–43.
[5] Friedman M, Byers SO, Roseman RH, Elevitch FR. Coronary-prone individuals (type A behavior pattern). Some biochemical characteristics. JAMA 1970;212(6):1030–7.
[6] Friedman M, Byers SO, Rosenman RH, Neuman R. Coronary-prone individuals (type A behavior pattern). Growth hormone responses. JAMA 1971;217(7):929–32.
[7] Friedman M, Rosenman RH. Type A behavior pattern: its association with coronary heart disease. Arn Clin Res 1971;3(6):300–12.
[8] McLachlan JF. A hostility scale for form R of the MMPI. J Clin Psychol 1974;30(3):369–71.
[9] Brazy JE, Lewis DV. Changes in cerebral blood volume and cytochrome aa3 during hypertensive peaks in preterm infants. J Pediatr 1986;108(6):983–7.
[10] Ferrari M, Giannini I, Sideri G, Zanette E. Continuous non invasive monitoring of human brain by near infrared spectroscopy. Adv Exp Med Biol 1985;191:873–82.

熱電運動素子を用いた完全埋め込み型人工心筋の開発*

伊吹竜太†, 円山重直†, 酒井清吾†, 山家智之‡, マスード・ベーニア§

Development of Totally Implant Artificial Heart Muscle Using Thermoelectric Actuator

Ryuta IBUKI†, Shigenao MARUYAMA†, Seigo SAKAI†, Tomoyuki YAMBE‡ and Masud BEHNIA§

Abstract

Thermoelectric actuator consists of shape memory alloy (SMA) and Peltier elements. Assemblage of these two functional materials is expected to realize compact and higher efficiency actuator. Utilize of thermoelectric cooling achieves quicker response. We made prototype actuator and evaluated its moving performance on both experiment and numerical simulation in order to apply thermoelectric actuator to heart pumping assist system. The actuator experimentally realizes 1 Hz motion in a circumstance assuming thermal condition in a human body. Numerical simulation using heat conduction equation including Peltier effect is carried out. Moving performance is expected to enhance if a junction between the Peltier element and electrode is improved. Realization about both structure with mechanical flexibility and resistance reducing on the junction is required in future improvement.

Key Words: *Thermoelectric Actuator, Thermoelectric Semiconductor, Shape Memory Alloys, Heat Conduction, Peltier Effect, Numerical Analysis*

記　号

A	:	断面積	[m^2]
c	:	比熱	[J/(Kg・K)]
h	:	熱伝達率	[W/m^2・K]
i	:	電流密度	[A/m^2]
I	:	電流	[A]
T	:	絶対温度	[K]
q	:	熱流束	[W/m^2]
κ	:	ゼーベック係数	[V/K]
λ	:	熱伝導率	[W/(m・K)]
ρ	:	密度	[Kg/m^3]
τ	:	時間	[s]
σ	:	電気伝導率	[$1/(\Omega \cdot m)$]

添　字

l	:	最外面（被覆表面）
f	:	周囲環境

1　緒　言

Ni-Ti 合金に代表される形状記憶合金（Shape Memory Alloy, SMA）は温度変化や応力変化によって異なる結晶構造を有する相へと転移し[1]、その際に生ずる特性は機能性材料として応用されている[2),(3]。外力によって応力誘起マルテンサイト相に変態する際に弾性定数が変化する「超弾性」[1]という性質は、携帯電話のアンテナ、めがねのフレームをはじめ、様々な用途に利用されている[2),(3]。また、一方で、低温で安定なマルテンサイト相状態において外力を加えて変形させても、高温時に安定な母相に

* Received : January 22, 2004, Editor : Mamoru OZAWA
† Institute of Fluid Science, Tohoku University (2-1-1, Katahira, Aoba-ku, Sendai, 980-8577, JAPAN)
‡ Institute of Development, Aging and Cancer Tohoku University (4-1, Seiryo, Aoba-ku, Sendai, 980-8575, JAPAN)
§ The University of Sydney (NSW 2006 AUSTRALIA)

なるよう相変態が開始する温度に加熱すると、変形前の形状に戻るという「形状記憶効果(shape memory effect)」[1]は、小型アクチュエータにおいてモーターに代わる動作機構として注目されている[2),(3)]。SMAを動作させる際、ジュール加熱を用いることで加熱時には比較的速い応答が得られる。一方で、対流に依る冷却速度は小さく、冷却速度向上のためには冷却装置の取り付けが必要不可欠である。

一方、ペルチェ素子は電流を流すことで熱を移動させることが可能な半導体デバイスで、動作部分を持たない冷却器として半導体レーザの温度制御などに応用されている[4]。低熱伝導率、高電気伝導度かつ高ゼーベック係数を有する素材は原理的に存在しないため、ペルチェ素子の定常冷却能力には限界がある。しかし、円山[5),(6)]はペルチェ素子の伝熱制御特性に注目し，ペルチェ素子を熱的に非定常な状態で動作させることによって、従来の定常性能に比べはるかに高い冷却能力が得られる非平衡熱電素子の原理を提唱し、航空機による微小重力実験における短時間急速冷却装置として応用している[6]。さらに円山ら[7]はこの非平衡熱電素子の原理を利用した形状記憶合金の急速加熱冷却によって動作する熱電運動素子を提案し、従来のアクチュエータと比べ高速で動作し、消費電力の小さな小型アクチュエータの実現性について報告を行っている。ペルチェ素子はヒートポンプとして動作するため、温度差が小さいときには投入電力以上の熱流束が得られ、高効率な加熱が可能である。

Thrasher[8] は Ni-Ti ワイヤーの加熱冷却サイクルについて数値計算による温度応答速度の比較を行っており、通電加熱と対流による冷却を用いた場合では 30 秒以上かかるサイクル周期を、ペルチェ素子による加熱冷却を用いることで 3.5 秒に短縮できるという結果を得ている。この他にも、ペルチェ素子と SMA を組み合わせたアクチュエータに関する研究[9)-(11)]がなされているが、いずれも SMA を電極代わりに利用しており、ペルチェ冷却の際に SMA の内部でジュール発熱が発生しており、冷却速度の低下を招いていると考えられる。

著者らは熱電運動素子を用いた人工補助心筋の開発研究を行っている。過去において Ti-Ni 合金を人工心臓へと応用する研究が Swayer[15]や仁田ら[16]によって行われたが、高い冷却速度が得られないことが問題となっていた。現在も医工学連携の下、Yambe ら[17]によって様々な人工心臓の開発がすすめられている。体外循環型の人工心臓システムを利用する場合、血液循環用の装置を常に体外に携帯し、ここから体内へとカニューレ(血液を輸送するパイプ)が患者の皮膚を貫いて心臓へと接続される。この場合、患者は症状によってはベッドから離れることができないとともに感染症の危険性に曝される。しかしこのような問題は、完全埋め込み型の人工心臓の利用によって解決できると考えられる。ところが、現在臨床試験が行われている完全埋め込み型人工心臓は一般的な東洋人の心臓に比べて大容量・大重量であるため、より小型の人工心臓が求められている。また、ポンプタイプの人工心臓では血栓が生じやすいという欠点がある。

これらを考慮に入れ、著者らは伸張屈曲を連続的に行う熱電運動素子を心筋に縫い付け、心臓の拍動が弱った際に動作し、拍動を活性化させる補助人工心筋の開発を目指している。このような補助人工心筋は一過性の発作や心臓移植手術におけるつなぎとして有効である。Matsuki ら[18),(19)]は体内に埋め込んだコイルに体外からコイルを当て、電磁誘導によって発電させた電力を小型バッテリーに充電するという経皮電力輸送システムの研究を行っている。これを人工心筋の駆動に必要な電力の供給に用いる予定である。このように、システム全体を患者の体内に埋め込むことで、患者は外見的には健常者と変わりなく生活を送ることが可能となる。

形状記憶効果による形状記憶合金の変位は変態温度域において著しい温度依存性を有する[2),(3)]。即ち、人工心筋の動作変位は SMA ロッドの温度変化に依存する。円山[5),(6)]はペルチェ素子を用いた急速冷却装置の解析に熱電効果を考慮に入れた非定常熱伝導方程式を用いている。この式に SMA ロッドの温度依存性を考慮することで、投入電力を入力として人工心筋内部の温度分布を求めることができる。さらに、この式と力学的負荷条件下における SMA ロッドの温度—ひずみ関係を組み合わせれば人工心筋の仕事効率を評価することも可能となる。

本論文では、実用化を目指した人工心筋用アクチュエータの開発のため、ペルチェ素子と SMA ロッドを組み合わせた熱電運動素子を用いた人工心筋を実際に製作し、力学的に無負荷条件下において、人工心筋に応用可能な高速動作に関する出力応答特性、人工心筋内部の非定常な温度変化特性について試作した人工心筋を用いて実験と数値計算により検証し、心臓を拍動するために必要な条件について検討した。

さらに、数値計算を用いて、性能向上のための改善点を指摘した。

2. 熱電運動素子の動作原理

Figure 1 は人工心筋用熱電運動素子の動作原理を示している。熱電運動素子を用いた人工心筋は熱電半導体、ヒートシンク、電極板、電気絶縁性フィルム、SMA ロッドによって構成される。一対の P および N 型半導体、電極板、ヒートシンクは直列に配置されペルチェ回路を形成している。電極と、高温域と低温域で形状記憶特性を有する全方位型 SMA の間に熱伝導性電気絶縁性のフィルムを配置することで、SMA には通電せず、SMA とペルチェ回路の間において熱だけが移動する構造とした。この構造において、SMA はペルチェ回路外に存在し、SMA の内部に電流は流れないのでジュール発熱しない。即ち、ペルチェ冷却による SMA の効率的な冷却が可能な構造とした。

P 型半導体と N 型半導体に電位差が生じると、ペルチェ効果による熱の移動がそれぞれの半導体の内部において発生する。電流の向きが逆転すると、ペルチェ効果による半導体内部の熱の移動方向が逆転するので、SMA は加熱（もしくは冷却）されることになる。

Ti-51at%Ni 製の SMA ロッドを、記憶したい形状（ここでは円弧状）に冶具を用いて拘束し、時効処理を施すと、全方位形状記憶効果を有するようになる。処理後の SMA ロッドは、常温以上の温度環境下において加熱すると、オーステナイト相変態温度域319－327Kにおいて顕著な形状変化を示す。また、加熱による変形後の SMA ロッドを冷却すると、中間相変態温度域約 324K から形状回復が開始し、約 316K でほぼ常温における形状に戻る。以下で述べる、相変態温度域は常温以上で SMA ロッドが顕著な変形を示す 316～327K とする。

この性質を利用し、ペルチェ回路に流れる電流の向きを連続的に切り替え、SMA を加熱冷却することで、SMA は反復動作を行うことが可能である。電極も兼ねた熱拡散率の高い銅製のヒートシンクは、ペルチェ素子から熱を効率よく吸収し、高速度な反復動作を実現させる。また、表面積の大きなヒートシンクを用いれば効率よく周囲環境へと放熱することができる。

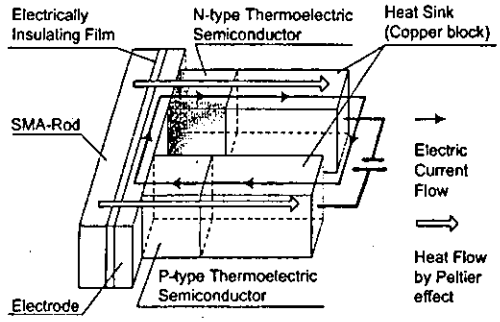

Fig.1 Moving concept of thermoelectric actuator

3. 人工心筋の構造

Figure 2 は人工心筋の構造概略図である。熱電半導体素子をヒートシンクと SMA の間に配置し、SMA とヒートシンクの間での熱量輸送をペルチェ効果によって行う。ペルチェ回路を形成するために、多数の P 型と N 型の熱電半導体素子が交互に配置されている。熱電半導体素子は電極を兼ねたヒートシンクとハンダ接合されている。一方、SMA ロッド上の銅製の電極と熱電半導体素子の接合は単純機械接触を用いることで、SMA ロッドが変形する際、接点にかかる応力を回避して SMA ロッドが柔軟に変形できる構造とした。両面が粘着性を有する熱伝導性電気絶縁性シートを電極と SMA ロッドの間に挟むことで両者を密着させて、電極と SMA ロッドとの間では電流は流れず、熱の移動のみが生ずる構造とした。電極とヒートシンクにより熱電半導体素子は直列に接合されており、その両端は外部電源と接続

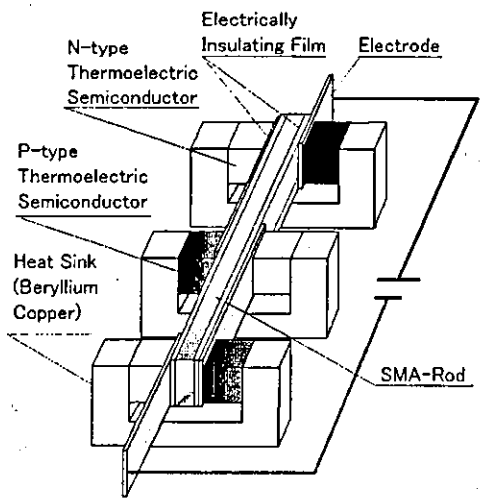

Fig.2 Structure of thermoelectric actuator

されている。熱電運動素子では、熱電半導体素子がSMA ロッドの両面に配置される直列回路を形成しており、一つ一つの半導体素子が立体的に組み上げられている。このような回路構造を構築することで、熱電運動素子ではSMA ロッドが効果的に加熱(電流方向が逆転すれば冷却)される。ヒートシンクの材質にばね性材料であるベリリウム銅を用い、その形状にはC型を採用した。これによりペルチェ素子と形状記憶合金を弾性的に挟み込むことが可能となり、密着固定による熱伝導の促進と構造の高耐久性を図った。

本報のペルチェ素子、SMA、ヒートシンクの配置は熱電運動素子の高速動作を目的としている。高速動作のためには、SMA ロッドの熱容量が小さく、熱電半導体素子ーSMA ロッド間の熱流束が大きい状態が望ましい。すなわち、SMA ロッドを外部環境から断熱し、ヒートシンクと外部環境の間での熱抵抗を小さくする必要がある。

Figure 3 は実際に製作した人工心筋で、全長100mm、直径5mm、重量15gと小型軽量である。

4 実験

Figure3 に示す試作した人工心筋を用いて、電流波形を印加した際の出力応答特性を実験により検証した。

4.1 実験方法

人工心筋の動作制御システムの構成を Fig.4 に示す。ファンクションジェネレータと電源装置を内蔵する制御コントローラを用いて正弦波形電圧の印加により、Fig.3 に示す人工心筋を動作させた。インキュベータを用いて 313.2K に保った電気絶縁性溶液中でラテックスゴムの膜で被覆した人工心筋を動作させることで、人体内温度環境での動作を模擬した。素線直径0.076mm のT型熱電対を SMA ロッド上と電気絶縁性溶液中に配置し、計測を行った。

4.2 実験結果

Figure 5 は、SMA ロッド表面の温度変化の典型的な計測結果を表している。SMA ロッドの温度変化は、正弦波形電圧印加直後、増加傾向を示しながら振動し、徐々に一定の振幅を保つようになる。その後、特定の温度域で温度上昇傾向は飽和し、上限温度と下限温度の間で安定した振幅を示した。

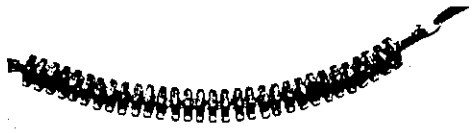

Fig.3 Artificial heart muscle using thermoelectric actuator, length: 100mm, diameter: 5mm, weight: 15g.

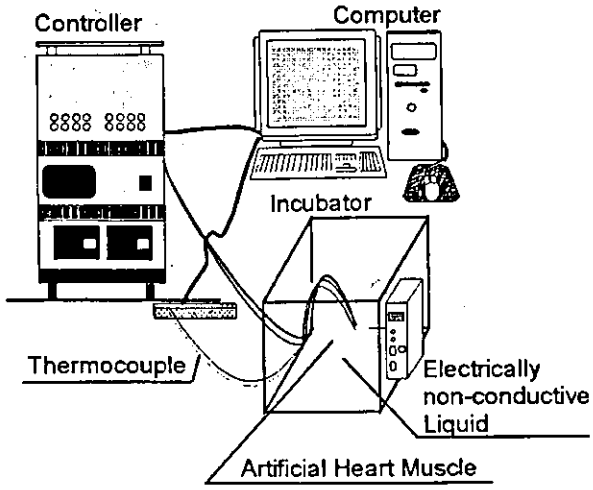

Fig.4 Artificial heart muscle control system

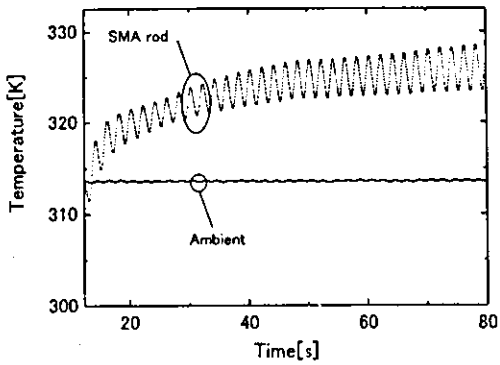

Fig.5 Experimental data of time dependent temperature variation on SMA rod (input electric wave: amplitude of voltage: V=±1.6V, electric current: I=1.1A, Frequency: f=0.5Hz, wave form: sine wave)

Table 1 に、入力波形をパラメータとして、SMA ロッドの温度上昇が飽和した状態についての値の中から代表的なものを示した。$T_{min.}$と$T_{max.}$はそれぞれ各入力値を与えた際に SMA の温度上昇が飽和した領域での温度振幅の上限温度と下限温度である。印加電圧の増加に伴い温度変化は大きくなる。しか

しながら、周波数 0.5Hz、振幅 2V では SMA ロッドの温度変化は相変態温度域より高温の領域で発生している。このような場合、SMA ロッドの歪量は変態温度域で発生するものよりも小さくなる。これは、印加した電流の増加に伴い、回路で生ずるジュール発熱がペルチェ効果による冷却を上回ったため SMA ロッドの温度が相変態温度域を上回ったためであると考えられる。このことを考慮すると、表中に示した入力値の中で最も大きな振幅が得られるのは 0.5Hz では 5.4K の温度変化が得られる 1.6V を印加した場合、1Hz では 1K の温度変化が得られる 1.3V を印加した場合である。又、この際の消費電力はいずれも 1W 以下に抑えられることが分かる。

変位計測システムを Fig.6 に示す。人工心筋を被覆するラテックスゴムの両端をアルミニウム板に固定し、レーザ変位計を用いて中央部分の動作変位を計測した。その結果、印加する電流波形の周波数 0.5Hz では約 0.5mm (SMA ロッドのひずみ 0.24%), 1Hz 動作では約 0.2mm(SMA ロッドのひずみ 0.1%) の最大変位を計測した。

5. 数値計算

非定常熱伝導方程式を用いた数値計算プログラムを開発し、これを用いて人工心筋内部の非定常な温度変化を理論的に検証した。また、このプログラムを用いた数値実験により人工心筋の性能向上のための改善点を指摘した。

5.1 計算モデル

人工心筋の構造を Fig.7 に示すモデルで一次元的に近似した。Fig.2 に示す熱電半導体の配置の採用により、SMA ロッドはペルチェ効果によって両側面から加熱もしくは冷却される。この際、人工心筋内部の伝熱は、ペルチェ効果が支配的と考えられるので、ペルチェ効果による熱の移動方向に一次元近似した。モデルは SMA ロッドの中央部からヒートシンクの外縁を覆うゴム膜までとし、各部品の物性値と断面積を位置の関数とした。

5.2 支配方程式

熱電効果を考慮に入れた支配方程式[5]は次式のようになる。

Table 1 Experimental value when time dependent temperature variation was saturated.

Input Wave			Ambient	SMA			Consumption
f[Hz]	E [V]	I [A]	T[K]	$T_{min.}$ [K]	$T_{max.}$ [K]	ΔT[K]	Power [W]
0.5	1.3	1	313.7	322.7	326.2	3.5	0.67
	1.6	1.1	313.7	325	330.4	5.4	0.88
	2	1.2	314.2	329.2	335.2	6	1.2
1	0.9	0.75	312.7	320.2	320.9	0.7	0.33
	1.1	1	312.2	321.7	322.5	0.8	0.53
	1.3	1.1	311.7	323.7	324.7	1	0.72

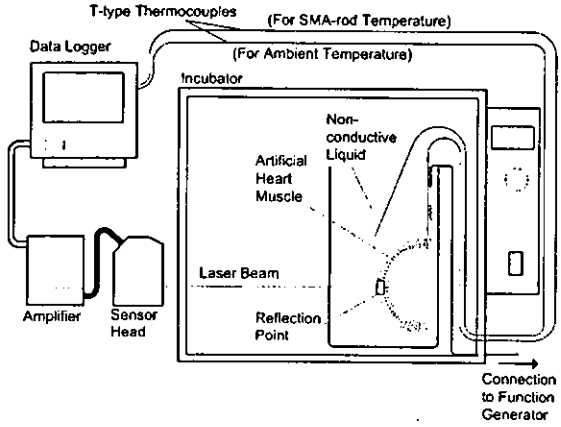

Fig.6 Displacement measurement system

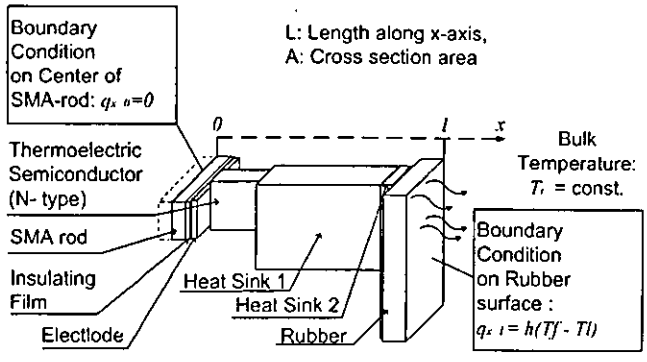

Fig.7 One-dimensional numerical model of artificial Muscle

$$Ac\rho\frac{\partial T}{\partial \tau} = \frac{\partial}{\partial x}\left(A\lambda\frac{\partial T}{\partial x} - A\kappa Ti\right) + Ai\kappa\frac{\partial T}{\partial x} + A\frac{i^2}{\sigma} \qquad (1)$$

右辺第 2,3,4 項はそれぞれペルチェ効果、ゼーベック効果、ジュール発熱に関する発熱項である。この式

を差分方程式に展開し、数値計算によって熱電半導体内部の非定常な温度変化を求めた。

5.3 初期条件、境界条件、物性値の温度依存性

初期条件を式(2)、境界条件を式(3),(4)に示す。

$$T(x)=T_f \quad (0\le x\le l) \tag{2}$$

$$\begin{cases} q_{x=0}=0 & (3) \\ q_{x=l}=h(T_f-T(l)) & (4) \end{cases}$$

境界条件は、SMA ロッドの中央部(x=0)において断熱、ゴム膜表面(x=l)において周囲環境流体との自然対流熱伝達を考慮した。そこで、人工心筋を被覆するゴム膜表面から電気絶縁性溶液中への熱伝達率を予備実験により求めるために予備実験を行った。その結果、h=240.2W/(m^2・K)を求め、この値を数値計算に使用した。

熱電半導体は温度に依存して物性値が変化するので上村、西田[4]の値を用いてこの温度依存性を考慮した。さらに SMA の相変態に伴う変態潜熱を数値計算において考慮するため、高木ら[20]の用いた比熱を温度の関数とする方法を採用し、相変態温度域において比熱の増加を考慮した。

5.4 接触抵抗

試作した人工心筋において、電極と熱電半導体間は単純機械接触しているため、接触熱抵抗と接触電気抵抗が存在している。そのため、実験結果と同様な温度履歴を得るためには数値計算モデルに接触面を考慮する必要がある。Figure 7 に示すモデルにおいて空気の層(熱容量:1184J/(m^{3}K) (空気 300K の値)、厚さ:1 μm) を電極と熱電半導体の間に追加し、これを接触面として考慮した。

接触熱抵抗の値は、接触面粗さと接触圧力から求める橘[21]の理論式を用いて 12K/W とした。さらに接触電気抵抗値を決定するため、接触電気抵抗値をパラメータとし SMA ロッド表面温度の時間変化について数値計算結果と実験結果を比較した。この際、両結果が最もよく近似した際に用いていた接触電気抵抗値を人工心筋の数値計算モデルに採用した。Figure 8 は振幅 1.2A, 周波数 1Hz の入力電流波形の場合に実験結果と数値計算結果を比較したものである。周囲環境温度は数値計算において一定とし、その値は実測値に近似した値を採用している。正弦波形状の電流波形を連続的に印加するという入力条件で計算を行った場合、Fig.5 に示す実験結果と同様に一定時間経過後に SMA ロッドの温度変化が定常状態に漸近し、ある温度域で安定な温度振幅が得られることを数値計算結果において確認することができた。この際の安定した温度振幅の大きさとその振幅の生じる温度域について実験結果と数値計算結果の比較を行い 17～25mΩの場合に Fig.8 に示すように両者の良い一致が得られた。この結果より、接触電気抵抗を 17mΩとして人工心筋の数値計算モデル化を行った。

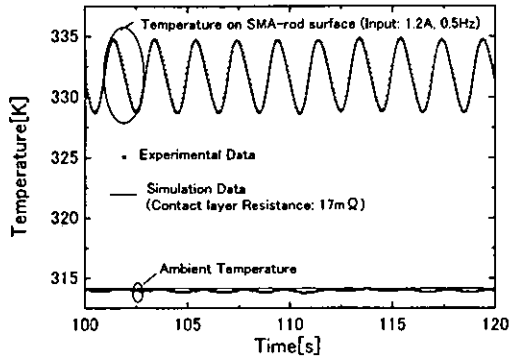

Fig.8 Comparison between both results of experiment and numerical simulation about time history of temperature on SMA-rod

5.5 数値計算結果

Figure 9 は、振幅 1A、周波数 1Hz の正弦波形電流を印加し、SMA ロッドの温度振幅が安定した時に得られる人工心筋内部の非定常な温度分布を 0.1s ごとに示したものである。SMA ロッドとペルチェ素子の間に位置する単純機械接触部分において不連続な温度分布が見られる。この結果において、SMA ロッドでの温度変化は 0.6K であった。

Figure9 の結果から単純機械接触部分の熱抵抗・電気抵抗が SMA ロッドの温度変化に与える影響が大きいものと考え、数値計算モデルにおいて熱電半導体 - 電極間の接触熱抵抗と接触電気抵抗の値が無視できるほど小さいと仮定した場合を数値計算により評価した。振幅 2A、周波数 1Hz の正弦波形電流を印加した場合の数値計算結果を Fig.10 に示す。この場合電極とペルチェ素子の間の温度変化は連続的になり、SMA ロッドにおける温度変化は 2.4K であった。

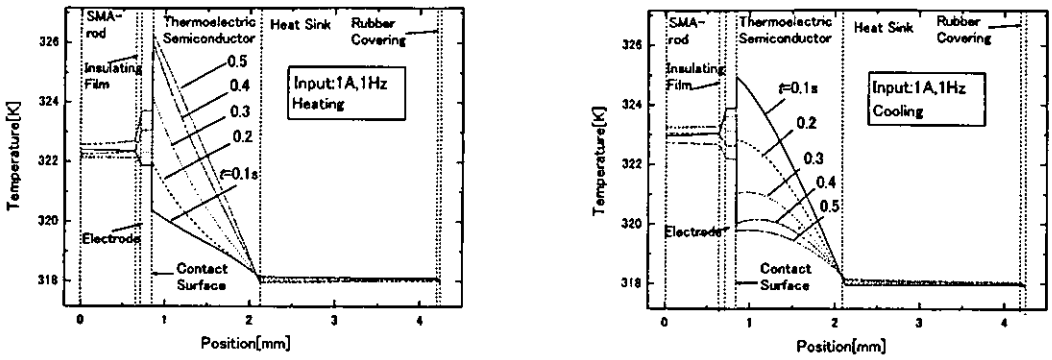

(a) (b)

Fig.10 Simulation results of time dependent temperature distribution about actuator inside when temperature variation on SMA rod is saturated. Connection condition between electrode and thermoelectric semiconductors: mechanical contact. (a) Heating and (b) cooling regime, Input electric wave: 1Hz, sine wave, amplitude: 1A. Ambient temperature: 314K.

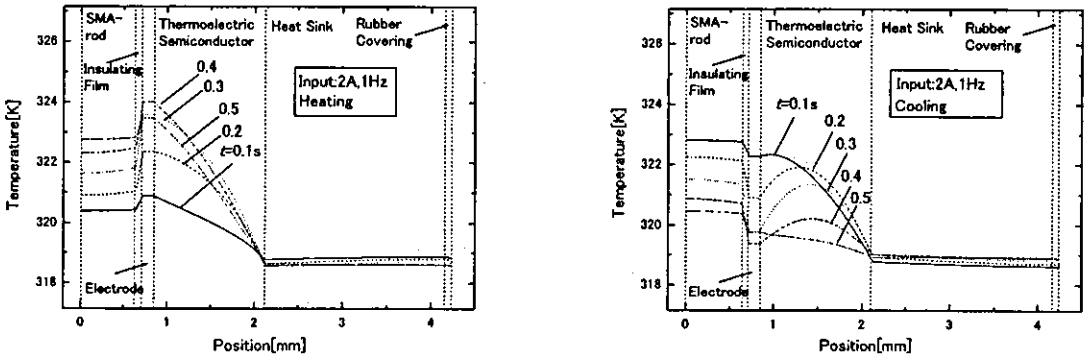

(a) (b)

Fig.11 Simulation results of time dependent temperature distribution about actuator inside when temperature variation on SMA rod is saturated. Connection condition between electrode and thermoelectric semiconductors: ideal connection. (a) Heating and (b) cooling regime, Input electric wave: 1Hz, sine wave, amplitude: 2A. Ambient temperature: 314K.

6. 性能向上のための改善点と今後の課題

実験と数値計算の結果から、人工心筋の動作性能向上のために構造上の改善点を検討した。

Table1 に示す 1Hz の波形電流を印加した実験結果において 1A 以上の電流を Fig.3 に示す人工心筋に印加すると、SMA ロッドの温度は相変態温度域を超えてしまう。しかし、Fig.10 の結果では 2A の印加でも、SMA ロッドの温度は相変態温度域内にとどまっている。この結果、次のような理由から、接触電気抵抗が人工心筋の性能低下を導いていると考えられる。ペルチェ効果は Eq.1 の右辺第 2 項に示すように電流値に比例して移動する熱量が増加する。一方で、ジュール発熱は Eq.1 の右辺第 4 項に示すように電流値の 2 乗に比例して増加する。即ち、電流の増加はペルチェ効果により温度変化量を増加させるが、接触電気抵抗がある場合では、ジュール加熱により SMA ロッドの温度を急激に上昇させる。

一方、Fig.9 の数値計算結果において、単純機械接触部分の不連続な温度変化は、接触熱抵抗のためにペルチェ素子から SMA ロッドへの伝熱量を抑制していると考えられる。そこで、各部品間の熱損失を低減させることで SMA ロッドに生ずる温度変化を大きくすることが可能であると考える。

これらの問題の改善方法として、電極、熱電半導体、ヒートシンク間の接合にはハンダ接合を用いて

電気抵抗と熱抵抗を低減する方法が考えられる。Abadie[22]もこの点に関して同様な考察を行っている。しかしながら、ハンダ接合によって部品を密着させてしまうことは、機械的な固定によって SMA の動作変位を抑制してしまうことにほかならない。そこで、これらの問題を解決する方法として、はんだ接合を用いながらも柔軟性を有する構造を現在検討している。

また、今後の課題として、以下の点を挙げる。

人体組織への熱の影響から、人工心筋に接する部分の温度は蛋白質の変質温度である 315K 以下に抑える必要がある。Figure.10 の結果では人体組織が接する部分に相当するゴム膜の温度が 318K であり、より低温に保つ必要がある。現在、放熱面積の大きなヒートシンクを使用することでゴム膜表面温度を低下させる方法を検討している。

実験によって得られた 1Hz での動作の最大変位は 0.2mm と、心臓の拍動を補助するには小さい。しかし、より小さな体積の SMA ロッドを使用すれば、熱容量が小さいので温度変化を増加させることが可能であり、変位を増加させることが可能であると考える。

今回の実験と数値計算はいずれも力学的に無負荷の条件下で行われたものである。実用時条件下での性能評価のため、今後、力学的負荷がかかった条件の下での変位測定や数値計算を行う予定である。

7. 結言

熱電半導体素子と形状記憶合金を組み合わせた熱電運動素子を用いた人工心筋の開発において、ペルチェ素子と SMA を組み合わせた熱電運動素子を用いた人工心筋を実際に製作し、その動特性を評価するために動作実験と数値計算を行い、以下に示す知見を得た。

1. 動作実験により、製作した人工心筋は人体内部を模擬した温度環境下において 1Hz の入力電流波形に対して、最大変位約 0.2mm での振動動作が可能であることを確認した。
2. 電極－熱電半導体素子間の接合状態を改善することで人工心筋の変位量が増加する可能性がある。
3. 補助人工心筋として熱電運動素子を応用するために、今後、動作変位の増加と人体組織に接する部分の温度低下が必要である。

参考文献

[1] *JIS H 7001, 形状記憶合金用語*, 財団邦人日本規格協会, (1989)

[2] 村上ほか, *形状記憶合金とその使い方*, 日刊工業新聞社, (1987)

[3] 舟久保ほか, *形状記憶合金*, 産業図書, (1984)

[4] 上村, 西田, *熱電半導体とその応用*, 日刊工業新聞社, (1988)

[5] 円山, *第 33 回日本伝熱シンポジウム公演論文集*, (1996), 127-128

[6] Maruyama, S., Nino, E. and Ruocco, G., *17th UIT National Heat Transfer Conference*, Vol. 2, (1999), 485-492.

[7] 円山, 小濱, 高木, *日本機械学会第 76 期全国大会講演論文集*(I), (1998), 327-328

[8] M. A. Thrasher, A. R. Shahin, P. H. Meckl, D. J. Jones, *1st European Conf. On Smart Structures and materials*, (1992), 197-200

[9] Potapov, P.L., *Materials Science and Engineering*, B52, (1998), 195-201

[10] Bhattachayya, A., Lagoudas, D.C., Wang, Y., and Kinra, V.K.,, *Smart Mater. Struct.* 4, (1995), 252-263

[11] Abadie, J., Chaillet, N. and Lexcellent, C., *Sensors and Actuators A: Physical*, 99-3, (2002), 297-303

[12] Maruyama, S., et al., *Int. J. Heat and Technology*, 19-2, (2002), 75-80

[13] Maruyama, S., et al., *Proc. of 20th UIT National Conference on Heat Transfer*, (2002), 443-448.

[14] Maruyama, S., et al., *Proc. of 12th International Heat Transfer Conference*, (2002),

[15] Sawyer, P.N. et al., *Trnas. Amer. Soc. Artif. Int. Organs*, 17, (1971), 470-473

[16] 仁田ほか, *信学技報*, MBE 83-49, (1983), 45-51

[17] Yambe T., et al., *Int. J. Artif. Organs*, 21-5, (1998), 279-284.

[18] Matsuki, H., et al., *J. Appl. Phys.* 64-10, (1988), 5859-5861.

[19] Matsuki, H., et al., *IEEE Trans. Magn.*, 26-1548, (1990), 1548-1550.

[20] 高木ほか, *日本機械学会論文集*, C, 63-615, (1997), 63-69.

[21] 橘, *日本機械学会誌*, 55-397, (1952), 102-107

[22] Abadie, J., et al., *Proc. of SPIE, Smart Struc. Mater.* 3667, (1999), 326–336.

INSTITUTE OF PHYSICS PUBLISHING JOURNAL OF MICROMECHANICS AND MICROENGINEERING
J. Micromech. Microeng. 15 (2005) 71–75 doi:10.1088/0960-1317/15/1/011

Ultra-miniature fiber-optic pressure sensor using white light interferometry

Kentaro Totsu[1], Yoichi Haga[2] and Masayoshi Esashi[3]

[1] Graduate School of Engineering, Tohoku University, 01 Aza-Aoba, Aramaki, Aoba-ku, Sendai 980-8579, Japan
[2] Tohoku University Biomedical Engineering Research Organization (TUBERO), 01 Aza-Aoba, Aramaki, Aoba-ku, Sendai 980-8579, Japan
[3] New Industry Creation Hatchery Center (NICHe), Tohoku University, 04 Aza-Aoba, Aramaki, Aoba-ku, Sendai 980-8579, Japan

E-mail: totsu@mems.mech.tohoku.ac.jp

Received 11 May 2004, in final form 2 August 2004
Published 8 October 2004
Online at stacks.iop.org/JMM/15/71

Abstract
We have developed a fiber-optic Fabry–Perot interferometric pressure sensor of 125 μm in diameter and a detection system for medical use. A Fabry–Perot cavity is formed at an optical fiber end. A deformation of the diaphragm of the Fabry–Perot cavity induced by pressure varies the cavity length. White light interferometry is used to avoid error and noise caused by bending of the optical fiber and fluctuation of the light source. The reflection light of the sensor cavity is detected by a commercial high-speed spectrometer. A pressure change has been detected by using the developed sensor system. Animal experiments using a goat have been carried out and dynamic pressure changes in the internal pressure of heart and aorta have been successfully monitored.

(Some figures in this article are in colour only in the electronic version)

1. Introduction

In medical diagnosis and treatment, pressure measurement is essential for monitoring the condition of a human body. Furthermore, the spread of minimally invasive therapy (e.g., percutaneous coronary intervention) requires monitoring local pressure in a very narrow space. To meet the demands, a miniaturized pressure sensor has been developed [1–6]. The pressure sensors utilize piezoresistive and optical detection using optical fibers. In particular, fiber-optic pressure sensors have the advantages of not only high potential of miniaturization but also applicability to use in such electromagnetically harsh environments as in an operating room in a hospital. Although small fiber-optic sensors have been commercialized, still it is difficult to meet the demands of the size and the shape. To realize the smallest and finest shape, a pressure sensor of 125 μm in diameter was developed in our research [7, 8]. The Fabry–Perot interferometric sensor the cavity length of which was changed by pressure was formed at the tip of the optical fiber. However, though the pressure sensor was small enough to install in interventional tools (e.g., catheter, guide wire), bending of the optical fiber and fluctuation of the laser diode used as the light source affected the sensor output. To reduce the effects of bending and fluctuation on the sensor output, a real-time measurement system which used spectrum modulation shifted by the distance change of the mirrors of the sensor cavity has been utilized. In this paper, we describe an ultra-miniature fiber-optic pressure sensor and a detection system for *in vivo* blood pressure monitoring.

2. Sensor system

The structure of the fiber-optic pressure sensor is shown in figure 1. The sensing element of 120 μm in diameter is composed of a thin silicon dioxide diaphragm with a mesa, an aluminum mirror on the mesa and a spacer fabricated by micromachining. It is bonded to the end of a multimode optical fiber. The outer diameter and the core diameter of the optical fiber are 125 μm and 50 μm, respectively. A chromium half-mirror is formed at the fiber end. A ring-shaped spacer made of polyimide (2 μm thick) is formed. The aluminum mirror and the chromium mirror spaced by the cavity constitute a

0960-1317/05/010071+05$30.00

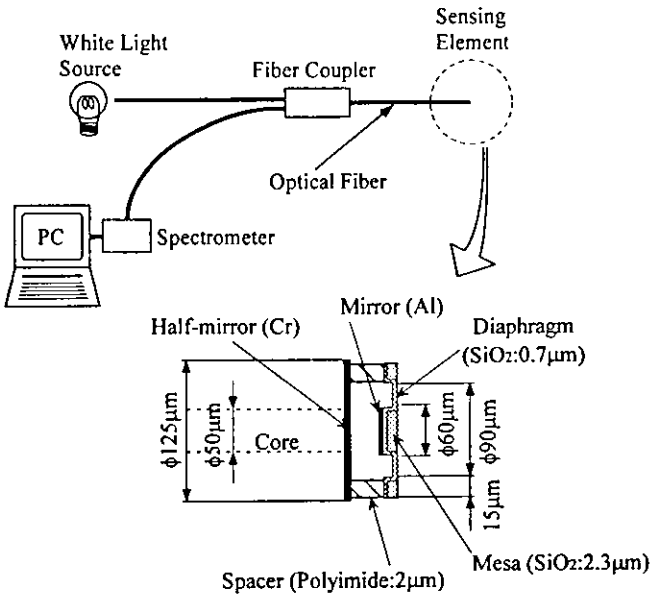

Figure 1. Schematic of sensor system.

Fabry–Perot interferometer (FPI) at the fiber end. The initial cavity length of the FPI is about 2 μm.

The deformation of the diaphragm induced by the pressure varies the cavity length. White light interferometry is utilized to detect the deformation of the diaphragm [9]. Low-coherence light from a white light source passes through the optical fiber to the sensor, and then the light is modulated at the FPI of the sensor. The light reflected by the sensor passes through the optical fiber again and is detected by a spectrometer. The cavity length d corresponding to applied pressure is determined by measuring the spectrum of the reflection light of the sensor. The cavity length d can be obtained by using

$$d = \frac{\lambda_1 \lambda_2}{2n(\lambda_2 - \lambda_1)}$$

where n represents the refractive index of the material of the sensor cavity, λ_1 and λ_2 represent adjacent peaks in the reflection spectrum [10].

Since the bending loss of the optical fibers and the fluctuation of the light source do not change the peak wavelengths of the spectrum but vary the total intensity of detected light, white light interferometry can reduce the influence of the bending loss and fluctuations on the output of the sensor system [11–14].

3. Sensor fabrication

The sensing element with a silicon column is batch fabricated on a silicon wafer by micromachining and is bonded to the half-mirror-coated optical fiber end utilizing patterned polyimide layer by thermocompression as shown in figure 2. After the bonding, unnecessary silicon column parts are removed by xenon difluoride (XeF_2) etching [8].

(a) Silicon dioxide film is deposited on both sides of a 200 μm thick silicon wafer by plasma-enhanced chemical vapor deposition (PECVD) using a tetraethoxysilane (TEOS) source. The film thickness of the top side is 2.3 μm and that of the bottom side is 1.2 μm. These silicon dioxide films are patterned for the mesa (top side) which keeps the aluminum reflecting mirror flat and the etching mask (bottom side) used in the later silicon deep reactive ion etching (deep RIE) process (e).

(b) Silicon dioxide film (0.7 μm thick) is deposited by atmospheric pressure chemical vapor deposition (APCVD) and is patterned.

(c) Aluminum is evaporated in vacuum and is patterned by a lift-off process for the reflecting mirror.

(d) Photosensitive-type polyimide (3 μm thick) is spin-coated and is patterned for the bonding layer and the spacer for the sensor interferometer.

(e) The silicon wafer is etched by silicon deep RIE. Then the sensing elements are released from the wafer.

(f) A thin chromium transparent layer as a half-mirror is coated on the end of the optical fiber in advance and the sensing element with the silicon column is bonded to the fiber end. Then the silicon part supporting the sensing element is etched by XeF_2.

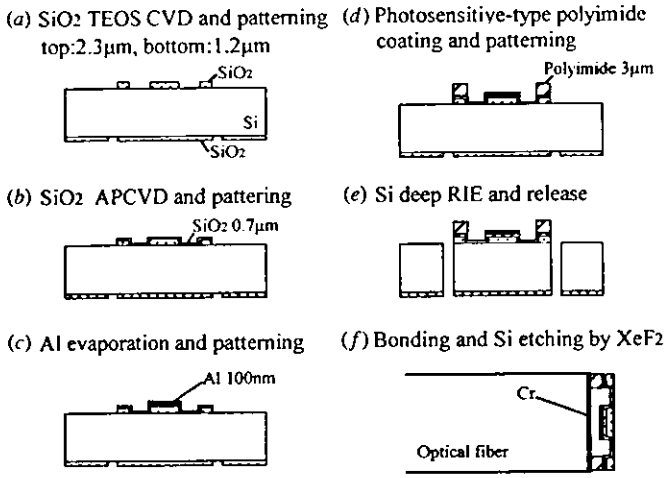

Figure 2. Schematic of the process for micromachined sensor structure.

Figure 3. Photograph of fabricated silicon columns with sensing element.

As the result of the fabrication process, many sensing elements with silicon column are batch fabricated as shown in figure 3. The diameter of the silicon column is 120 μm, and the length is 200 μm, which is almost equal to the wafer thickness. Approximately 100 000 pieces of sensor elements